UAV-Aided ISAC with A Rotatable Dipole Array: Joint Beamforming and Steering Optimization

Fengcheng Pei, Anja Klein, and Lin Xiang
Communications Engineering Lab, Technical University of Darmstadt, Germany
Email: {f.pei, a.klein, l.xiang}@nt.tu-darmstadt.de

***Abstract*—In this paper, we consider integrated sensing and communication (ISAC) enabled by an unmanned aerial vehicle (UAV) hovering at a fixed position in the air. Unlike previous works, the UAV is equipped with a rotatable uniform linear array (ULA) of half-wavelength dipole antennas. This configuration allows for adaptive adjustments of beamforming, array orientation, and the radiation pattern of the dipoles to enable efficient sensing of multiple targets while maintaining communication with multiple users. Our goal is to maximize the sum of transmit beampattern gains towards all sensing targets, while ensuring quality-of-service (QoS) for each communication user through the joint optimization of beamforming and three-dimensional (3D) array steering. The formulated problem is highly nonconvex, presenting significant challenges in obtaining its solution. To address this, we employ a proximal block coordinate descent (BCD) method to decompose the problem into several low-complexity convex and manifold optimization subproblems. Simulation results demonstrate the substantial advantages of joint beamforming and array steering with the proposed rotatable dipole antenna array in UAV-aided ISAC, especially in complex ISAC environments.**

I. Introduction

Unmanned aerial vehicles (UAVs) provide a flexible platform for enabling sensing and communication applications in non-terrestrial networks (NTNs) in the sixth-generation (6G) era [1]. Thanks to their agile mobility and flexible deployments, UAVs can extend network coverage and enhance sensing and communication services in both terrestrial and satellite networks. Building on the momentum of integrated sensing and communication (ISAC) research in terrestrial 6G networks, UAV-aided ISAC has recently attracted significant attention [2]. However, existing solutions are often ill-suited for UAV-aided ISAC, due to the unique channel characteristics and resource constraints of UAVs, which differ from those of terrestrial nodes. How to craft the ISAC design tailored for UAVs and optimize the UAV-aided ISAC system remains a compelling and open challenge in 6G research [3].

In this paper, we focus on the design and optimization of UAV-aided ISAC using a multi-antenna transmitter. Since ISAC relies on a shared transmitter to send a common signal for sensing and communication functions, a multi-antenna transmitter can provide abundant spatial degrees-of-freedom (DoFs) to meet the requirements of both tasks [4]. However, UAVs are usually constrained by size, weight and power (SWAP), which limits the feasibility of deploying large antenna arrays onboard. To address this limitation, prior research has explored the joint optimization of beamforming and trajectory design for UAV-aided ISAC, aiming to leverage the UAV's three-dimensional (3D) mobility to create a distributed, virtually large antenna array across time and space. In [5]–[7], the authors jointly optimized the transmit beamforming of a uniform linear array (ULA) and the UAV's trajectory to maximize the communication throughput while maintaining beampattern gains above a specified threshold for each sensing target. However, these studies [5]–[7] assumed ideal isotropic antennas in ULAs, neglecting the 3D radiation patterns of real-world antennas.

Recently, UAV-enabled wireless networks employing arrays of directional antennas have attracted significant interest [8]–[11]. In [8], the optimal directivity factor was investigated for balancing sensing coverage and network connectivity. Additionally, [9] evaluated the impact of vertical and horizontal configurations of a dipole antenna array in UAV-based localization. However, both studies [8], [9] assumed *fixed* orientations for the antenna arrays throughout their analyses. In [10], we proposed a novel multi-antenna transmitter enabled by a *rotatable* antenna array for UAV-aided ISAC. Specifically, the UAV employs a ULA composed of practical patch antennas, which can be mechanically steered/rotated in 3D space, either through UAV movement or an onboard gimbal. By jointly leveraging the 3D radiation pattern of patch antennas, array steering, and beamforming, we can generate highly directive beams for communication users/sensing targets to enhance the reception of desired signals in the main lobe, reduce power leakage in the side lobes, and/or minimize interference or clutter interception. In [11], we further explored the use of the rotatable array for UAV-aided ISAC in a bistatic radar setup. Both transmit beamforming and array steering are optimized to maximize the received sensing power while ensuring quality-of-service (QoS) for each communication user.

Unlike previous studies [8]–[11], this paper investigates UAV-aided ISAC using a rotatable ULA composed of half-wavelength dipoles, whose radiation patterns differ significantly from those of patch antennas. Specifically, dipoles radiate in all directions within the plane perpendicular to the antenna axis, making them suitable for applications requiring wide-area coverage, whereas patch antennas only radiate into half space. Due to this difference, the performance limits of rotatable dipole array have to be newly investigated. To address this, we jointly optimize beamforming and 3D steering of the dipole array to maximize the total power radiated towards multiple sensing targets while ensuring QoS for multiple communication users. Furthermore, unlike [10], [11], which focused solely on optimizing beamforming directions, we

This work has been funded by the LOEWE initiative (Hesse, Germany) within the emergenCITY center under grant LOEWE/1/12/519/03/05.001(0016)/72 and has been supported by the BMBF project Open6GHub under grant 16KISKO14 and by DAAD with funds from the German Federal Ministry of Education and Research (BMBF).

additionally optimize the power of each beamforming vector.

Due to the directional radiation pattern of dipoles and the 3D steering of the dipole array, the resulting optimization problem is highly nonconvex and generally intractable. By exploring the underlying structure of the problem, we decompose it into multiple manifold and convex optimization subproblems. Based on this, we further propose a low-complexity iterative algorithm to solve these subproblems. Our contributions are:

- We investigate UAV-aided ISAC utilizing a rotatable ULA composed of dipole antennas, and we jointly optimize the beamforming and array steering to increase the performance gains.
- We formulate a non-convex problem to maximize the sum of transmit beampattern gains towards all the targets and ensure QoS for each communication user, and we propose a low-complexity proximal block coordinate descent (BCD) method to solve it.
- Simulation results verify that joint optimization of beamforming and array steering in a dipole antenna array markedly surpasses the performance of using an isotropic antenna array in enhancing the attainable region for sensing and communication. This superiority is attributed to the high directivity of the dipole array and the added rotational degrees of freedom (DoFs).

Notation: In this paper, matrices and vectors are represented by boldface capital and lower-case letters, respectively. $\mathbb{C}^{m\times n}$ and $\mathbb{R}^{m\times n}$ denote $m\times n$ complex- and real-valued matrices, respectively. $j=\sqrt{-1}$ is the imaginary unit and $\|\cdot\|$ is the l_2-norm of a vector. $\boldsymbol{A}^T$ and $\boldsymbol{A}^H$ are the transpose and complex conjugate transpose of matrix $\boldsymbol{A}$, respectively. $\mathrm{tr}(\boldsymbol{A})$ and $\mathrm{rank}(\boldsymbol{A})$ denote the trace and rank of matrix $\boldsymbol{A}$, respectively. Finally, $\overrightarrow{\boldsymbol{a}}$ denotes the unit direction vector.

The structures of the remainder of the paper is as follows. The system model is introduced in Section II. The optimization problem is formulated and solved in Sections III and IV, respectively. Section V gives the simulation results and finally, Section VI concludes the paper.

II. System Model

In this section, we introduce the signal and channel models of the system. As shown in Fig. 1, we consider an ISAC system enabled by a rotary-wing UAV. The UAV hovers at a fixed position $P=(x,y,H)$ and serves as an aerial access point (AP) to simultaneously provide communication and sensing services for multiple terrestrial users and multiple targets indexed by sets $\mathcal{K}=\{1,...,K\}$ and $\mathcal{L}=\{1,...,L\}$, respectively. The positions of user $k\in\mathcal{K}$ and target $l\in\mathcal{L}$, denoted by $P_{U,k}=(x_k,y_k,z_k)$ and $P_{T,l}=(x_l,y_l,z_l)$, respectively, are assumed to be known at the UAV a priori. We equip the UAV with a ULA composed of N half-wavelength dipole antennas. By mounting the dipole array on the UAV with a gimbal, the orientations of both the dipole elements and the array can be flexibly adjusted in 3D space. Fig. 1 illustrates the dipole array in green solid line segments. Each communication user employs a single receive antenna.

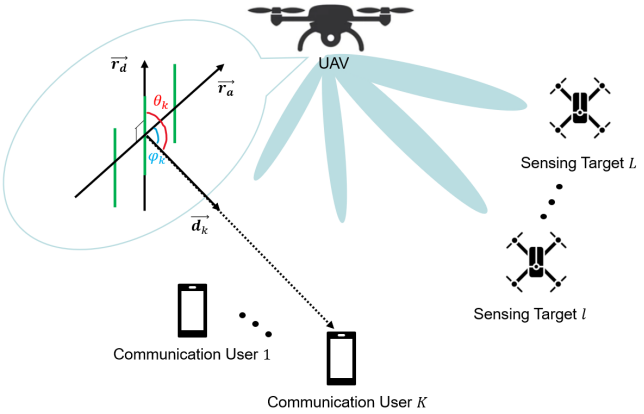

Fig. 1. System model of UAV-aided ISAC.

A. Channel Model and 3D Steering of Dipole Array

We assume that the hovering UAV experiences strong LoS channels to all users and targets [6]. Then, the channel vector $\boldsymbol{h}_k$ between the UAV and communication user k is modeled as

$$\boldsymbol{h}_k=\frac{\sqrt{\beta}}{D_k}\cdot\boldsymbol{a}_{U,k}, \tag{1}$$

where β is the reference value of power-wise path loss at unit distance, $D_k=\sqrt{(x_k-x)^2+(y_k-y)^2+(z_k-H)^2}$ denotes the distance between the UAV and user k, and $\boldsymbol{a}_{U,k}\in\mathbb{C}^{N\times 1}$ is the steering vector of the transmit antenna array towards user k.

Considering the 3D radiation pattern of the dipole array, the steering vector $\boldsymbol{a}_{U,k}$ can be modeled as [13]

$$\boldsymbol{a}_{U,k}=\alpha\cdot\mathrm{E}(\theta_k)\cdot\mathrm{A}(\varphi_k). \tag{2}$$

$\mathrm{E}(\theta_k)$ and $\mathrm{A}(\varphi_k)$ denote the element factor of a single dipole antenna and the array factor, respectively. θ_k and φ_k represent the angles of departure seen from user k with respect to (w.r.t.) the dipole axis and the array axis, respectively. We refer to θ_k and φ_k as the elevation angle and azimuth angle of user k, respectively, for convenience. Fig. 1 depicts θ_k and φ_k in red and blue arcs, respectively. Assuming that all communication users and sensing targets are located in the far field of the dipole array, the element factor $\mathrm{E}(\theta_k)$ in (2) admits a closed-form expression given by

$$\mathrm{E}(\theta_k)=\frac{\cos\left(\frac{\pi}{2}\cos\theta_k\right)}{\sin\theta_k}, \tag{3}$$

and the array factor $\mathrm{A}(\varphi_k)$ is expressed as

$$\mathrm{A}(\varphi_k)=(1,e^{j\frac{2\pi}{\lambda}d\cos\varphi_k},\cdots,e^{j(N-1)\frac{2\pi}{\lambda}d\cos\varphi_k})^T, \tag{4}$$

where λ is the transmit carrier wavelength and d is the spacing between adjacent dipoles in the array. Finally, α is a normalization coefficient to limit the total radiated power, where $\frac{1}{2\pi}\int_0^{2\pi}\mathrm{E}^2(\theta_k)d\theta_k=1$.

However, constrained by the geometry of the dipole array as shown in Fig. 1, θ_k and φ_k cannot be adjust independently during array steering, since they both depend on the orientation of the antenna array. To enable a convenient model of the

3D array steering, we further define two orthonormal vectors $\{\overrightarrow{\boldsymbol{r}_a}, \overrightarrow{\boldsymbol{r}_d}\}$. As shown in Fig. 1, vectors $\overrightarrow{\boldsymbol{r}_a} \in \mathbb{R}^{3\times 1}$ and $\overrightarrow{\boldsymbol{r}_d} \in \mathbb{R}^{3\times 1}$ denote the directions of the array's axis and dipole antennas, respectively. Moreover, let $\overrightarrow{\boldsymbol{d}_k} \in \mathbb{R}^{3\times 1}$ be the unit direction vector of user k seen from the UAV and defined by $\overrightarrow{\boldsymbol{d}_k} \triangleq (x_k - x, y_k - y, z_k - H)^T / D_k$. Thus, vector $\overrightarrow{\boldsymbol{d}_k}$ forms an angle φ_k w.r.t. $\overrightarrow{\boldsymbol{r}_a}$ and another angle θ_k w.r.t. $\overrightarrow{\boldsymbol{r}_d}$, respectively. Using the defined direction vectors, the impact of array steering on θ_k and φ_k can be captured by

$$\varphi_k = \arccos(\overrightarrow{\boldsymbol{d}_k}^T \cdot \overrightarrow{\boldsymbol{r}_a}) \tag{5}$$

$$\theta_k = \arccos(\overrightarrow{\boldsymbol{d}_k}^T \cdot \overrightarrow{\boldsymbol{r}_d}). \tag{6}$$

Therefore, we can flexibly adjust vectors $\{\overrightarrow{\boldsymbol{r}_a}, \overrightarrow{\boldsymbol{r}_d}\}$ in 3D space for steering the dipole array.

B. ISAC Signal Model and Transmit Beampattern

Let $s_k \in \mathbb{C}$ denote the data symbol intended for user $k \in \mathcal{K}$. We assume that s_k is a complex Gaussian random variable with zero mean and unit variance, i.e., $s_k \sim \mathcal{CN}(0, 1)$. For information transmission, the UAV sends the transmit signal

$$\boldsymbol{s} = \sum\nolimits_{k=1}^{K} \boldsymbol{w}_k \cdot s_k \tag{7}$$

over the dipole array, where $\boldsymbol{w}_k \in \mathbb{C}^{N\times 1}$ is the transmit beamforming vector for user k. The received signal at user k is given as

$$y_k = \boldsymbol{h}_k^H \cdot \boldsymbol{s} + n_k, \tag{8}$$

where $n_k \in \mathbb{C}$ is the receiver noise power at user k and is modeled as a zero-mean Gaussian random variable with variance σ_k^2, i.e., $n_k \sim \mathcal{CN}(0, \sigma_k^2)$. Based on (8), the maximum achievable rate of user k in bps/Hz is given as

$$R_k = \log_2\left(1 + \text{SINR}_k\right), \tag{9}$$

$$\text{SINR}_k = \frac{|\boldsymbol{h}_k^H \boldsymbol{w}_k|^2}{\sum_{m=1, m\neq k}^{K} |\boldsymbol{h}_k^H \boldsymbol{w}_m|^2 + \sigma_k^2}, \tag{10}$$

where SINR_k denotes the signal-to-interference-plus-noise ratio (SINR) of user k.

Meanwhile, the UAV (which acts as a monostatic radar sensor) or another bistatic receiver collects echos of the transmit signal $\boldsymbol{s}$ that are reflected or scattered by the targets. These echos are processed for sensing purpose, such as to detect the presence and/or track the location of the targets. Please refer to [11] and [12] for detailed modeling of echo signal reception and processing. However, in order to focus on transmit beamforming design in this paper, we consider the transmit beampattern gain towards sensing target l as the sensing performance metric, which is given as

$$G_{T,l} = \sum\nolimits_{k=1}^{K} \left|\boldsymbol{w}_k^H \boldsymbol{a}_{T,l}\right|^2. \tag{11}$$

Here, $\boldsymbol{a}_{T,l} \in \mathbb{C}^{N\times 1}$ denotes the steering vector of the transmit dipole antenna array towards target l. $\boldsymbol{a}_{T,l}$ can be modeled in the same manner as $\boldsymbol{a}_{U,k}$ by replacing the angle pairs $\{\varphi_k, \theta_k\}$ in (2) with $\{\varphi_l, \theta_l\}$. Using (11), a detailed modeling of the sensing receiver can be ignored, which also eliminate the signaling overhead for synchronizing/coordinating the UAV transmitter and the sensing receivers as well as estimating the channel conditions between them.

III. Problem Formulation

Both the achievable data rate of each communication user in (9) and the transmit beampattern gain towards each target in (11) depend on the beamforming vector $\boldsymbol{w}_k$ and the orientation $\{\overrightarrow{\boldsymbol{r}_a}, \overrightarrow{\boldsymbol{r}_d}\}$ of the dipole array, which need to be intelligently designed for the multi-antenna transmitter of UAV-aided ISAC. To this end, we jointly optimize the beamforming and array steering to maximize the sum of radiated sensing power, measured by the weighted sum of transmit beampattern gains towards all targets, while guaranteeing given QoS requirements for each communication user. The resulting optimization problem is formulated as

$$\begin{aligned} \underset{\boldsymbol{w}_k, \overrightarrow{\boldsymbol{r}_a}, \overrightarrow{\boldsymbol{r}_d}}{\text{maximize}} \quad & \sum\nolimits_{l=1}^{L} c_l G_{T,l} \\ \text{subject to} \quad & \text{C1: } \sum\nolimits_{k=1}^{K} \|\boldsymbol{w}_k\|^2 \leq P_{\max}, \\ & \text{C2: } \text{SINR}_k \geq r_k, \ k \in \mathcal{K}, \\ & \text{C3: } \left\|\overrightarrow{\boldsymbol{r}_a}\right\| = 1, \\ & \text{C4: } \left\|\overrightarrow{\boldsymbol{r}_d}\right\| = 1, \\ & \text{C5: } \overrightarrow{\boldsymbol{r}_a} \cdot \overrightarrow{\boldsymbol{r}_d} = 0. \end{aligned} \tag{P1}$$

In (P1), $c_l \geq 0$ denotes the weight of transmit beampattern gain towards target l, where $\sum_{l=1}^{L} c_l = 1$. Constraint C1 limits the UAV's total transmit power by $P_{\max}$. The QoS constraint C2 guarantees a minimum received SINR of r_k, or equivalently a minimum data rate of $\log_2(1 + r_k)$ in bps/Hz, for each communication user k. Constraints C3, C4 and C5 capture 3D array-steering using orthonormal unit vectors $\{\overrightarrow{\boldsymbol{r}_a}, \overrightarrow{\boldsymbol{r}_d}\}$, cf. Fig. 1.

In problem (P1), both the objective function and the constraints C2, C3, C4 and C5 are nonconvex. Hence, (P1) is a highly non-convex problem formulation that is generally NP-hard. Besides, beamforming vector $\boldsymbol{w}_k$ and array steering $\{\overrightarrow{\boldsymbol{r}_a}, \overrightarrow{\boldsymbol{r}_d}\}$ are tightly coupled in the objective function and in the constraint C2, rendering the problem even more challenging to solve. In the next section, we will propose a low-complexity algorithm to decompose (P1) into several convex or manifold subproblems, and optimize the beamforming and array steering iteratively.

IV. Problem Solution

We observe that constraints C1 and C2 possess underlying convex properties, and constraints C3, C4 and C5 construct a special manifold. Leveraging the inherent structures of the problem, we propose an iterative proximal BCD algorithm [14] to decompose problem (P1) into three subproblems, each of which optimizes one of the three variable blocks, namely $\{\boldsymbol{w}_k\}$, $\{\overrightarrow{\boldsymbol{r}_a}\}$, and $\{\overrightarrow{\boldsymbol{r}_d}\}$, while keeping the other two blocks of variables fixed. Furthermore, we also introduce proximal and penalty terms to improve the convergence of the algorithm and independently address the optimization of beamforming and array steering in the subproblems of (P1), respectively.

A. Subproblem for Optimizing Beamforming Vector $\boldsymbol{w}_k$

When fixing array steering $\{\overrightarrow{\boldsymbol{r}_a}, \overrightarrow{\boldsymbol{r}_d}\}$, the subproblem for optimizing the beamformer $\boldsymbol{w}_k$ for given transmit power budget and communication QoS is defined as

$$\begin{aligned} \underset{\boldsymbol{w}_k \in \mathbb{C}^{N\times 1}}{\text{maximize}} \quad & \sum\nolimits_{l=1}^{L} c_l G_{T,l} \\ \text{subject to} \quad & \text{C1}, \\ & \overline{\text{C2}}\text{:} \ \sum\nolimits_{m=1,m\neq k}^{K} r_k \cdot |\boldsymbol{h}_k^H \boldsymbol{w}_m|^2 \\ & - |\boldsymbol{h}_k^H \boldsymbol{w}_k|^2 + r_k \cdot \sigma_k^2 \leq 0, \ k \in \mathcal{K}. \end{aligned} \tag{P2}$$

Note that in (P2), constraint C2 is rewritten as $\overline{\text{C2}}$ with a quadratic form, which makes (P2) a quadratically constrained quadratic program (QCQP) and can be sovled by semidefinite programming (SDP) relaxation. We define a new optimization variable $\boldsymbol{X}_k \triangleq \boldsymbol{w}_k \boldsymbol{w}_k^H$, where $\boldsymbol{X}_k \in \mathbb{C}^{N\times N}$ is a symmetric and positive semidefinite matrix with rank one. Then (P2) can be equivalently reformulated as

$$\begin{aligned} \underset{\boldsymbol{X}_k \in \mathbb{C}^{N\times N}}{\text{maximize}} \quad & \sum\nolimits_{l=1}^{L} c_l \sum\nolimits_{k=1}^{K} \text{tr}(\boldsymbol{A}_{T,l} \boldsymbol{X}_k) \\ \text{subject to} \quad & \overline{\text{C1}}\text{:} \ \sum\nolimits_{k=1}^{K} \text{tr}(\boldsymbol{X}_k) \leq P_{\max} \\ & \widetilde{\text{C2}}\text{:} \ \sum_{m\neq k} r_k \cdot \text{tr}(\boldsymbol{H}_k \boldsymbol{X}_m) - \text{tr}(\boldsymbol{H}_k \boldsymbol{X}_k) + r_k \sigma_k^2 \leq 0 \\ & \text{C6}\text{:} \ \boldsymbol{X}_k \succeq \boldsymbol{0}, \\ & \text{C7}\text{:} \ \text{rank}(\boldsymbol{X}_k) = 1, k \in \mathcal{K}, \end{aligned} \tag{P3}$$

where $\boldsymbol{A}_{T,l} \triangleq \boldsymbol{a}_{T,l} \boldsymbol{a}_{T,l}^H$ and $\boldsymbol{H}_k \triangleq \boldsymbol{h}_k \boldsymbol{h}_k^H$. Problem P3 remains NP-hard due to the non-convex nature of the rank constraint C7. Nevertheless, by relaxing C7, the resultant problem transforms into a convex one, which can then be efficiently addressed using available solvers, such as CVX [15]. In general, the relaxed problem of (P3) may not always lead to a rank-one solution, i.e., $\text{rank}(\boldsymbol{X}_k^*) \neq 1$. Additional steps such as Gaussian randomization or Eigen Value decomposition are needed to recover optimal $\boldsymbol{w}_k^*$ from $\boldsymbol{X}_k^*$ [16].

B. Subproblem for Optimizing 3D Array Steering

It remains to optimize the array steering $\{\overrightarrow{\boldsymbol{r}_a}, \overrightarrow{\boldsymbol{r}_d}\}$ with beamforming vector $\boldsymbol{w}_k$ being fixed. In the following, we only show the solution for the subproblem of optimizing $\overrightarrow{\boldsymbol{r}_a}$. Exploiting the symmetry between $\overrightarrow{\boldsymbol{r}_a}$ and $\overrightarrow{\boldsymbol{r}_d}$, the subproblem of optimizing $\overrightarrow{\boldsymbol{r}_d}$ can then be tackled by simply interchanging $\overrightarrow{\boldsymbol{r}_a}$ and $\overrightarrow{\boldsymbol{r}_d}$ in the presented solution.

Considering the mechanical structure of the ULA composed of dipole antennas as shown in Fig. 1, when we fix the unit vector $\overrightarrow{\boldsymbol{r}_d}$, the vector $\overrightarrow{\boldsymbol{r}_a}$ will be on a unit circle manifold within the null-space of $\overrightarrow{\boldsymbol{r}_d}$, which inspires us to employ manifold optimization. Manifold optimization is concerned with the optimization problem

$$\min_{x\in\mathcal{M}} g(x), \tag{12}$$

where $\mathcal{M}$ is a Riemannian manifold and g is a real-valued function on $\mathcal{M}$. If additional constraints other than the manifold constraint are involved, such as the QoS constraints here, we can add in g an indicator function of the feasible set of these additional constraints. Therefore, the subproblem of optimizing $\overrightarrow{\boldsymbol{r}_a}$ is formulated as

$$\begin{aligned} \underset{\overrightarrow{\boldsymbol{r}_a} \in \mathbb{R}^{3\times 1}}{\text{minimize}} \quad & -\sum\nolimits_{l=1}^{L} c_l G_{T,l} + c \cdot \|\overrightarrow{\boldsymbol{r}_a} - \overrightarrow{\boldsymbol{r}_a}'\|^2 \\ & + \rho \cdot \sum\nolimits_{k=1}^{K} u \log(1 + e^{\frac{r_k - \text{SINR}_k}{u}}) \\ \text{subject to} \quad & \text{C3}, \text{C5}. \end{aligned} \tag{P4}$$

Observe that the original maximization problem in (P1) has been reformulated into a minimization problem through the inversion of the sign in the objective function. $c \geq 0$, $\rho > 0$ are penalty factors and $u > 0$ is the smoothing factor. $\overrightarrow{\boldsymbol{r}_a}'$ represents the direction vector obtained in the preceding iteration and $c \cdot \|\overrightarrow{\boldsymbol{r}_a} - \overrightarrow{\boldsymbol{r}_a}'\|^2$ is a quadratic proximal term, which is employed to enhance convergence of the iterations by connvexifing problem (P4) and imposing penalties on substantial deviations between the optimal solution of (P4) and $\overrightarrow{\boldsymbol{r}_a}'$. We also eliminate constraint C2 by introducing a weighted exact penalty $\rho \cdot \sum_{k=1}^{K} u \log(1 + e^{\frac{r_k - \text{SINR}_k}{u}})$ for preventing violations. The residual constraints C3 and C5 construct a specific manifold, namely, a unit circle, and then problem (P4) can be solved by the Riemannian conjugate gradient (RCG) method based manifold optimization [17].

In order to keep consistency between Problem (P4) and (12), we now transfer C3 and C5 into a unit circle manifold constraint. We denote the objective function of (P4) by $f(\overrightarrow{\boldsymbol{r}_a})$ and define $\boldsymbol{e} = [\boldsymbol{e}_1, \boldsymbol{e}_2] \in \mathbb{R}^{3\times 2}$ as the orthonormal basis for the null-space of $\overrightarrow{\boldsymbol{r}_d}$. So we can substitute the optimization variable $\overrightarrow{\boldsymbol{r}_a}$ in (P4) by

$$\overrightarrow{\boldsymbol{r}_a} = \boldsymbol{e} \cdot \boldsymbol{\gamma}_a, \tag{13}$$

where $\boldsymbol{\gamma}_a \in \mathbb{R}^{2\times 1}$ is the new optimization variable with $\|\boldsymbol{\gamma}_a\| = 1$. As a result, (P4) is reformulated as

$$\begin{aligned} \underset{\boldsymbol{\gamma}_a \in \mathbb{R}^{2\times 1}}{\text{minimize}} \quad & f(\boldsymbol{e} \cdot \boldsymbol{\gamma}_a) \\ \text{subject to} \quad & \text{C8}\text{:} \ \|\boldsymbol{\gamma}_a\| = 1. \end{aligned} \tag{$\overline{\text{P4}}$}$$

Problem ($\overline{\text{P4}}$) can be solved with off-the-shelf solvers such as pymanopt using RCG [17]. The selection of the penalty weight

Algorithm 1 REPMS for solving problem ($\overline{\text{P4}}$)

Input: Initial $\boldsymbol{\gamma}_{a,0}^*$, initial penalty weight ρ_0, initial smoothing factor u_0, $\delta_\rho > 1$, $0 < \delta_u < 1$, $u_{\min}$, $\rho_{\max}$, stopping threshold ϵ, $q_0 = \left\|\boldsymbol{\gamma}_{a,0}\right\|$ and $t = 0$

Output: Optimal $\boldsymbol{\gamma}_a^*$

1: **while** $q_t > \epsilon$ **do**
2: Optimize problem ($\overline{\text{P4}}$) with $\rho = \rho_t$ and $u = u_t$ by RCG manifold optimization, and get $\boldsymbol{\gamma}_{a,t+1}^*$.
3: $\rho_{t+1} \leftarrow \min\{\delta_\rho \rho_t, \rho_{\max}\}$.
4: $u_{t+1} \leftarrow \max\{\delta_u u_t, u_{\min}\}$.
5: $q_{t+1} \leftarrow \left\|\boldsymbol{\gamma}_{a,t+1}^* - \boldsymbol{\gamma}_{a,t}^*\right\|$.
6: $t \leftarrow t + 1$.
7: **end while**

ρ requires careful consideration, as an excessively large value of ρ can result in an ill-conditioned problem within ($\overline{\text{P4}}$) and impede the algorithm's convergence rate. A practical approach is to set a relatively small initial value for ρ, optimize $\boldsymbol{\gamma}_a$ in ($\overline{\text{P4}}$), and iteratively increase ρ and re-optimize [18]. The overall algorithm for solving ($\overline{\text{P4}}$), known as the Riemannian exact penalty method via smoothing (REPMS), is summarized in Algorithm 1, and optimal $\overrightarrow{\boldsymbol{r}}_a^*$ can be achieved by (13).

The overall approach to addressing problem (P1) is iteratively optimizing the three variable blocks $\{\boldsymbol{w}_k\}$, $\{\overrightarrow{\boldsymbol{r}}_a\}$, $\{\overrightarrow{\boldsymbol{r}}_d\}$ until the convergence is achieved.

V. Simulation Results

In this section, the performance of the proposed scheme for UAV-aided ISAC is evaluated through simulations. We consider a UAV equipped with a rotatable ULA composed of 8 half-wavelength dipole antennas. The UAV hovers at position $(20, 20, 20)$ for the dual purpose of communicating with $K = 2$ users and sensing $L = 3$ targets in the 30 GHz frequency band, where the wavelength is $\lambda = 10$ mm. User 1 is located at $P_{U,1} = (-90, 620, 0)$ and user 2 is located at $P_{U,2} = (130, 620, 0)$. The targets are situated in close proximity of the UAV, where target 1 is located at $P_{T,1} = (26, 21, 10)$, target 2 is located at $P_{T,2} = (15, 24, 25)$ and target 3 is located at $P_{T,3} = (16, 21, 20)$. Neighboring dipole elements are separated by $d = \frac{\lambda}{2}$ and the maximal transmit power of the UAV is $P_{\max} = 2$ W. The minimum required SINR r_k is set to 1 for all users, guaranteeing a minimum data rate of $\log_2(1 + r_k) = 1$ bps/Hz per user. The upper bound of penalty factor $\rho_{\max}$ and the lower bound of smoothing factor $u_{\min}$ are set to 10^6 and 10^{-6} [18], respectively. The initial array steering is given by $\overrightarrow{\boldsymbol{r}}_{a,0} = (1, 0, 0)^T$ and $\overrightarrow{\boldsymbol{r}}_{d,0} = (0, 0, 1)^T$. Finally, the noise power and the path loss coefficient are set as $\sigma_k^2 = 10^{-12}$ W, $k \in \mathcal{K}$, and $\beta = 10^{-6}$, respectively. For performance comparison, we consider the following schemes as benchmarks,

- *Baseline Scheme 1:* The UAV employs a rotatable ULA of isotropic elements. The array steering and beamforming are jointly optimized using the proposed proximal BCD.
- *Baseline Scheme 2:* The UAV employs a non-rotatable ULA with isotropic elements with fixed array steering $\overrightarrow{\boldsymbol{r}}_a = (1, 0, 0)^T$. Only the beamforming will be optimized.

Owing to the omni-directional radiation pattern characteristic of isotropic antennas, the orientation of the ULA composed of such antennas can be sufficiently described by the direction of the array's axis alone, namely, the unit vector $\overrightarrow{\boldsymbol{r}}_a$.

Fig. 2 depicts the optimized transmit beampattern gains of all schemes, and illustrates how our proposed UAV-aided ISAC using a rotatable ULA of dipole antennas outperforms the baseline schemes. The dashed lines represent the normalized azimuth angle, φ_k/π, of each user or target relative to the UAV's array orientation vector $\overrightarrow{\boldsymbol{r}}_a$. When using a non-rotatable ULA of isotropic antennas for UAV-aided ISAC, the users and targets are located at widely dispersed azimuth angles w.r.t. the initial array orientation $\overrightarrow{\boldsymbol{r}}_a = (1, 0, 0)^T$ as depicted in Fig. 2(a). We observe that Baseline Scheme 2 distributes the beams among all the targets and communication users, and this distribution results in diminished sensing power for each target, since only the electrical beamforming is optimized. In contrast, with array steering, Baseline Scheme 1 can co-align users and targets into the same beam as shown in Fig. 2(b), where user 1, target 1 and target 2 are aligned into a singular, high-gain beam, improving the sensing performance. When utilizing the proposed rotatable ULA of dipole antennas, different transmit beampattern gains are observed by each target or user as denoted by variously colored curves, due to the directional radiation pattern of dipole antennas. We find that the proposed scheme aligns the targets and users not only in the azimuth angle, but also in the elevation angle as shown in Fig. 2(c), where the transmit beampattern gains of different users and targets are nearly overlapping. Moreover, the dipole antenna-based ULA generates beams of markedly higher strength than those from a ULA of isotropic antennas, owing to the directivity of the dipole elements. As a result, the proposed scheme effectively leverages the beamforming, rotational DoFs, and high directivity of dipoles to achieve the best performance.

Fig. 3(a) and Fig. 3(b) evaluate the sum of transmit beampattern gains directed towards the targets achieved with the considered schemes for varying minimum data rates requested by the users and varying number of transmit antennas, respectively. From Fig. 3(a), we observe that Baseline Schemes 1 and 2 exhibit a significant reduction in sum of beampattern gains with increasing minimum data rates, especially beyond 3 bps/Hz, due to the trade-off between sensing efficiency and communication QoS under a given power budget. Significantly, Baseline Schemes 1 and 2 fail to meet the minimum data rates requirements beyond 4.5 bps/Hz and 4.2 bps/Hz, respectively. This is primarily due to the challenging nature of our ISAC scenario, which involves widely spaced user and target locations, demonstrating a considerable challenge for the ULA composed of isotropic elements. Through the array steering, Baseline Scheme 1 achieves a sensing performance gain of approximately 2.0 dBi compared to Baseline Scheme 2. This improvement is credited to the capability to modify the azimuth angles of both users and targets with Baseline Scheme 1, as illustrated in Fig. 2(b), which in turn enhances the beamforming efficiency of the ULA. Besides, Fig. 3(a) indicates that using a rotatable ULA with dipole antennas results in a notably superior sensing performance compared to Baseline Scheme 1, achieving an increased gain relative to the Baseline 1 with 3.6 dBi and 7.9 dBi for lower and higher data rates, respectively. Figure 3(b) demonstrates that across all considered schemes, there is an enhancement in sensing performance with the increase of the number of transmit antennas, due to the increased spatial DoFs that can be utilized in beamforming. To sum up, the proposed scheme is suitable for ISAC scenarios involving widely spaced targets and users, or those requiring high minimum data rates, and it also has the potential for applications in UAVs with SWAP constraints, since the proposed scheme already achieves significantly high performance even with a small number of antennas.

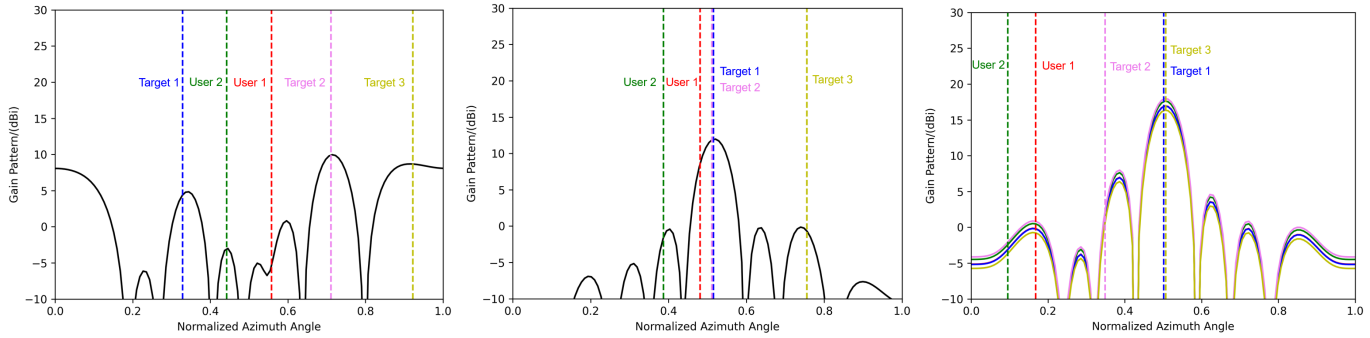

(a) (b) (c)

Fig. 2. Optimized Beampattern Gains of (a) Baseline 2, (b) Baseline 1, and (c) Proposed scheme.

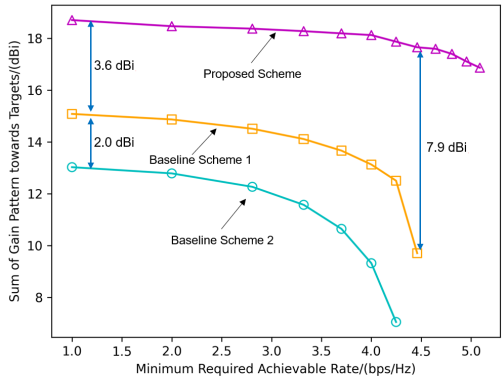

(a)

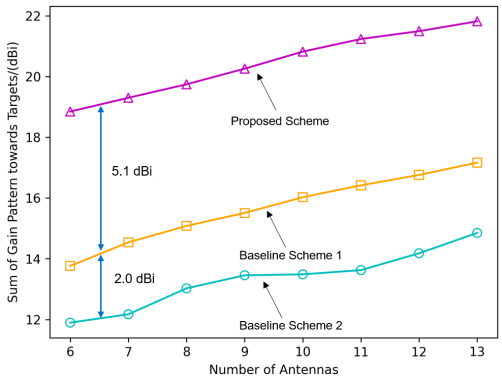

(b)

Fig. 3. Performance comparison of considered schemes for (a) increasing minimum required data rates of users and (b) increasing number of antennas.

VI. Conclusions and Future Work

In this paper, we explore joint optimization of beamforming and 3D array steering using a rotatable ULA composed of half-wavelength dipole antennas for UAV-aided ISAC, where the UAV hovers at a fixed position in the air. The formulated problem to maximize the sum of transmit beampattern gains towards all targets and guarantee QoS for each communcation user is highly non-convex, and we decompose it into several low-complexity convex and manifold optimization subproblems with the proximal BCD method. Simulation results verify that with beamforming and array steering, the proposed ULA of dipole antennas demonstrates superior performance in complex ISAC environments, excelling even in scenarios with limited number of transmit antennas. Our future studies will focus on the joint optimization of beamforming, array steering, and UAV flight trajectory in UAV-aided integrated sensing and communication.

References

[1] M. A. Khan, et al., "Swarm of UAVs for Network Management in 6G: A Technical Review," *IEEE Transactions on Network and Service Management*, vol. 20, no. 1, pp. 741-761, March 2023.

[2] O. Rezaei, M. M. Naghsh, et al., "Resource Allocation for UAV-Enabled Integrated Sensing and Communication (ISAC) via Multi-Objective Optimization," *IEEE International Conference on Acoustics, Speech and Signal Processing (ICASSP)*, pp. 1-5, 2023.

[3] J. Mu, R. Zhang, et al., "UAV Meets Integrated Sensing and Communication: Challenges and Future Directions," *IEEE Communications Magazine*, vol. 61, no. 5, pp. 62-67, May 2023.

[4] J. A. Zhang et al., "Enabling Joint Communication and Radar Sensing in Mobile Networks—A Survey," *IEEE Commun. Surveys & Tut.*, vol. 24, no. 1, pp. 306-345, 1st quarter 2022.

[5] K. Meng, Q. Wu, et al., "UAV Trajectory and Beamforming Optimization for Integrated Periodic Sensing and Communication," *IEEE Wireless Commun. Lett.*, vol. 11, no. 6, pp. 1211-1215, Jun. 2022.

[6] K. Meng, Q. Wu, et al., "Throughput Maximization for UAV-Enabled Integrated Periodic Sensing and Communication," *IEEE Transactions on Wireless Communications*, vol. 22, no. 1, pp. 671-687, Jan. 2023.

[7] Q. Wu, Y. Zeng, et al., "Joint Trajectory and Communication Design for Multi-UAV Enabled Wireless Networks," *IEEE Trans. Wireless Commun.*, vol. 17, no. 3, pp. 2109-2121, Mar. 2018.

[8] J. Peng, W. Tang and H. Zhang, "Directional Antennas Modeling and Coverage Analysis of UAV-Assisted Networks," *IEEE Wireless Commun. Lett.*, vol. 11, no. 10, pp. 2175-2179, Oct. 2022.

[9] P. Sinha and I. Guvenc, "Impact of Antenna Pattern on TOA Based 3D UAV Localization Using a Terrestrial Sensor Network," *IEEE Trans. Veh. Techno.*, vol. 71, no. 7, pp. 7703-7718, Jul. 2022.

[10] F. Pei, L. Xiang and A. Klein, "Joint Optimization of Beamforming and 3D Array-Steering for UAV-Aided ISAC," *ICC 2024 - IEEE International Conference on Communications*, Denver, CO, USA, 2024, pp. 1249-1254.

[11] Pei, F., Xiang, L. and Klein, A. "Transmit Beamforming and Array Steering Optimization for UAV-Aided Bistatic ISAC", *IEEE Global Communications Conference*, Cape Town, South Africa, 2024.

[12] Yilmaz, B., Klein, A. and Xiang, L. "Energy Minimization for UAV-Aided ISAC in A Cluttered Environment", in Proc. IEEE Globecom workshops, Cape Town, South Africa, Dec. 2024.

[13] C. A. Balanis, *Antenna Theory: Analysis and Design*. John Wiley & Sons, 4th ed, 2016.

[14] J. Bolte, S. Sabach and M. Teboulle, "Proximal alternating linearized minimization for nonconvex and nonsmooth problems," *Mathematical Programming*, vol. 146, no. 1-2, pp. 459-494, Oct. 2014.

[15] S. Boyd and L. Vandenberghe, *Convex Optimization*. Cambridge University Press, 2004.

[16] D. P. Palomar and Y. C. Eldar, *Convex Optimization in Signal Processing and Communications,* 2009.

[17] P.-A. Absil, R. Mahony and R. Sepulchre, *Optimization Algorithms on Matrix Manifolds.* Princeton University Press, 2009.

[18] C. Liu and N. Boumal, *Simple algorithms for optimization on Riemannian manifolds with constraints*. Jan. 2019.